Theory of plasmons in carbon nanotube bundles



2002 J. Phys.: Condens. Matter 14 5239

(http://iopscience.iop.org/0953-8984/14/20/319)

INSTITUTE OF PHYSICS PUBLISHING JOURNAL OF PHYSICS: CONDENSED MATTER

J. Phys.: Condens. Matter **14** (2002) 5239–5253 PII: S0953-8984(02)33804-9

# Theory of plasmons in carbon nanotube bundles

**William Que**

MPCS, Ryerson University, 350 Victoria Street, Toronto, Ontario, Canada M5B 2K3

E-mail: wque@ryerson.ca

Received 14 February 2002
Published 9 May 2002
Online at stacks.iop.org/JPhysCM/14/5239

**Abstract**

We develop a suitable theoretical framework for studying plasmons in nanotube bundles. In the plane perpendicular to the tubes, the nanotubes form a two-dimensional lattice. We use a simple model of free electron gas confined to arrays of cylindrical surfaces, however the theoretical framework can also be applied to more sophisticated models for carbon nanotubes. Both intrasubband (classical) and intersubband (quantum) plasmons in such nanotube bundle systems are studied. Analytical solutions have been obtained for the case where only one subband is occupied, while numerical solutions have been obtained for the case of many occupied subbands. Intertube Coulomb coupling is found to play an intricate role, as it can both harden and soften plasmon modes in the same nanotube bundle. Intertube Coulomb coupling is also responsible for sizable plasmon dispersions in the transverse plane. All plasmons are found to be undamped by the corresponding single particle type electron–hole pair excitations. The classical plasmon exhibits three-dimensional character in the long wavelength limit, and one-dimensional character in the short wavelength limit. For quantum plasmons, the plasmon energy can be significantly larger than the corresponding single particle excitation energy between subbands. This feature is similar to quantum plasmons in semiconductor quantum wire systems.

## 1. Introduction

Since the discovery of carbon nanotubes in 1991 by Iijima [1], the study of carbon nanotube systems has been an active area of research. These cylindrical fullerenes are molecular versions of quantum wires with a very rich portfolio of mechanical structures and interesting electrical and optical properties [2]. Many applications of carbon nanotubes are possible, from artificial muscles [3], molecular electronics [4], to data storage, field emission displays and sensors. Li *et al* [5] have successfully grown highly ordered hexagonal arrays of carbon nanotubes.

Plasmon excitations in a single carbon nanotube have been studied by several authors theoretically. Sato *et al* [6] derived the general expression for the dielectric function for a

  

single walled nanotube, and gave analytical and numerical results for the intrasubband plasmon. Davids *et al* [7] presented numerical results for intersubband plasmons. Lin *et al* [8,9] studied both intrasubband and intersubband plasmons in both single walled and multiwalled carbon nanotubes. Others [10, 11] have also presented similar studies. Magnetoplasmons in a single carbon nanotube have been studied by several authors as well [12–14].

A number of experimental papers on plasmons in carbon nanotubes detected by electron energy loss spectroscopy (EELS) have also been published [15–18]. These papers identified bulk plasmons [16–18] as well as a surface plasmon [15]. The lower energy mode in the 5–8 eV range has been identified as the $\pi$ plasmon, while the higher energy mode in the 20–30 eV range has been identified as the $\pi + \sigma$ plasmon. Momentum dependent EELS measurements by Knupfer *et al* [18] found significant dispersion of the $\pi$ plasmon.

For a single carbon nanotube, the cylindrical symmetry of the tube greatly simplifies the problem, implying that there is no coupling between plasmon modes of different azimuthal indices. In a periodic array of carbon nanotubes, the cylindrical symmetry is broken by intertube Coulomb coupling, and in general the dielectric matrix has nonzero off-diagonal elements and the plasmon modes become coupled. Lin *et al* [19–22] have extended their theoretical study to a carbon nanotube lateral lattice (a periodic array where the nanotubes form a one-dimensional (1D) array in the plane transverse to the direction of the tubes), and to carbon nanotube bundles, where a two-dimensional (2D) lattice is formed in the plane transverse to the direction of the tubes [23, 24]. However, while the authors seem to have done a fine job in the case of a single nanotube, the extensions of their theory to periodic arrays have suffered from serious problems. In [19] the authors found the intersubband plasmon to be an acoustic mode. This result is unphysical because the intersubband plasmon energy should not be less than the single particle intersubband transition energy in the long wavelength limit. Indeed, in similar systems of semiconductor quantum wire arrays, the fact that intersubband plasmons are optical modes are well established [25,26]. When dealing with wavevector conservation in periodic arrays, Lin *et al* [19–23] have neglected umklapp terms which have been found to play a crucial role for intersubband plasmons in semiconductor quantum wire arrays [25,26]. At zero wavevector, the umklapp terms make a nonzero, substantial contribution in the intersubband part of the dielectric function. The expressions in [21–23] for the dielectric function in the small wavevector limit are meaningless, because the zeroth order term due to umklapp contribution absent from the expressions actually dominates over the terms dependent on the wavevector. In [24], Huang *et al* kept the umklapp terms in the initial formalism, however the authors worked with a dielectric function in reciprocal lattice space, which in principle requires the solving of an $n \times n$ matrix where $n$ is infinite. In the actual calculations, the authors kept only the term corresponding to a null reciprocal lattice vector, making the approximation equivalent to [21–23]. Based on the work on semiconductor quantum wire arrays [25], it is known that the convergence in reciprocal lattice space is slow. From the work presented in this paper, we can infer that if the formalism of [24] is used, a matrix size of about $640\,000 \times 640\,000$ is needed to achieve convergence for a carbon nanotube bundle (the authors truncated the matrix to $1 \times 1$). In this paper, we show that the formalism can be developed without spanning the dielectric function in reciprocal lattice space, eliminating the need to use such large matrices.

The aim of this paper is to develop a suitable theoretical framework for plasmons in a carbon nanotube bundle, or a carbon nanotube array which forms a 2D lattice in the plane perpendicular to the nanotubes. Real samples like this with a hexagonal lattice in the transverse plane have been fabricated [5]. The interplay between the azimuthal symmetry of a single tube and the azimuthal symmetry breaking by the intertube Coulomb coupling, and the symmetry of the 2D lattice make this system much more complex and interesting than a single nanotube. We model electrons in the conduction band of carbon nanotubes as electron gas confined to

cylindrical shells. This is an over simplification, because in real carbon nanotubes there are $\pi$ band and $\sigma$ band electrons, and the electronic properties are dependent on the geometric arrangement of atoms on the carbon nanotube. Ostling *et al* [27] find that a jellium model can account for the most essential features of the electronic structure in carbon nanotube systems. The electron gas model allows us to concentrate on developing a correct theoretical framework. Once the framework is established, it can be combined with more realistic electronic band states for more quantitative comparison with experiments. We expect results from this paper to be qualitatively correct for the $\pi$ plasmon. The $\pi + \sigma$ plasmon found experimentally cannot be described in the present work since it will require a two species electron gas model or real electronic band structure. The theoretical framework in this paper can be extended to deal with these issues in the future.

## 2. Formalism

We consider a carbon nanotube bundle whose cross section is a 2D lattice. To study collective electronic excitations in the system, we use the self-consistent field formalism of Ehrenreich and Cohen [28], neglecting retardation effects. This formalism, combined with a quantum mechanical treatment, has been applied successfully to quantum wire superlattices [25, 26] and quantum dot arrays [29]. This approach has the advantage that both intrasubband and intersubband plasmons can be studied on the same footing.

In this paper we need to use both 2D and 3D vectors. Three-dimensional vectors are indicated by bold letters, while 2D vectors are indicated by a bar on top.

We start from the Poisson equation in Fourier space

$$V(\boldsymbol{q}) = \frac{4\pi e^2}{\epsilon q^2} n(\boldsymbol{q}) \tag{2.1}$$

where $\boldsymbol{q}$ is a 3D wavevector, $\epsilon$ is the background dielectric constant, $V(\boldsymbol{q})$ is the Coulomb potential, and $n(\boldsymbol{q})$ is the density response. If we represent single particle quantum electronic states in a lattice of carbon nanotubes as $|a\rangle$, $n(\boldsymbol{q})$ can be expressed as

$$n(\boldsymbol{q}) = 2 \sum_{a,a'} \langle a|V|a'\rangle \langle a'|\mathrm{e}^{\mathrm{i}\boldsymbol{q}\cdot\boldsymbol{r}}|a\rangle \frac{f_{a'} - f_a}{E_{a'} - E_a + \hbar\omega} \tag{2.2}$$

where $a, a'$ are composite quantum numbers for the spatial degrees of freedom, $f_{a'}$, $f_a$ are Fermi distribution functions, and $E_{a'}$, $E_a$ are single particle energies. The factor of 2 in equation (2.2) comes from spin degeneracy since we assume no magnetic field is applied. The matrix element for the Coulomb potential $V(\boldsymbol{r})$ can be rewritten as

$$\langle a|V|a'\rangle = \sum_{\boldsymbol{q}'} V(\boldsymbol{q}') \langle a|e^{-\mathrm{i}\boldsymbol{q}'\cdot\boldsymbol{r}}|a'\rangle \tag{2.3}$$

where we have made use of the Fourier expansion for $V(\boldsymbol{r})$.

For a lattice of nanotubes where overlap of wavefunctions between different nanotubes is small, it is an excellent approximation to replace $|a\rangle$ with a tight-binding wavefunction,

$$|a\rangle = \mathrm{e}^{\mathrm{i}k_z z} \sum_{\bar{r}_j} \psi_m(\bar{\rho} - \bar{r}_j) \mathrm{e}^{\mathrm{i}\bar{k}\cdot\bar{r}_j}. \tag{2.4}$$

Here we have assumed that the nanotubes are aligned in the $z$ direction and form a 2D lattice in the transverse plane. Hence $\bar{r}_j$ is the 2D lattice vector, and $\bar{\rho}$ is the projection of the 3D vector $\boldsymbol{r}$ onto the transverse plane.

In this paper we treat carbon nanotubes as cylindrical shells of radius $R$ with negligible wall thickness. Due to the cylindrical symmetry of a carbon nanotube, the wavefunction $\psi_m(\bar{\rho})$ has the form

$$\psi_m(\bar{\rho}) = f(\rho)\mathrm{e}^{\mathrm{i}m\phi}, \qquad m = 0, \pm 1, \pm 2, \ldots, \tag{2.5}$$

where $\phi$ is the azimuthal angle, and $f(\rho)$ is related to the $\delta$-function by

$$2\pi\rho f^2(\rho) = \delta(\rho - R). \tag{2.6}$$

The single particle energy $E_a$ is given by

$$E_{k_z,m} = \frac{\hbar^2 k_z^2}{2m^*} + \frac{\hbar^2 m^2}{2m^* R^2}, \tag{2.7}$$

where $m^*$ is the effective mass of the electron.

Making use of equation (2.4) and neglect wavefunction overlap between different nanotubes, we obtain

$$\langle a'|\mathrm{e}^{\mathrm{i}\boldsymbol{q}\cdot\boldsymbol{r}}|a\rangle = \delta_{k_z',k_z+q_z}\delta_{\bar{k}',\bar{k}+\bar{q}_{xy}+\bar{G}}A_{mm'}(\bar{q}_{xy}) \tag{2.8}$$

where $\bar{G}$ is a 2D reciprocal lattice vector, and

$$A_{mm'}(\bar{q}_{xy}) = \int\int \psi^*_{m'}(\bar{\rho})\psi_m(\bar{\rho})\mathrm{e}^{\mathrm{i}\bar{q}_{xy}\cdot\bar{\rho}}\rho\,\mathrm{d}\rho\,\mathrm{d}\phi = \frac{1}{2\pi}\int_0^{2\pi}\mathrm{e}^{\mathrm{i}(m-m')\phi}\mathrm{e}^{\mathrm{i}q_{xy}R\cos(\phi-\phi_0)}\,\mathrm{d}\phi. \tag{2.9}$$

In the above equation, $\phi_0 = \arctan(q_y/q_x)$, $q_{xy} = \sqrt{q_x^2 + q_y^2}$. Since

$$\mathrm{e}^{\mathrm{i}x\cos\phi} = \sum_{n=-\infty}^{\infty}\mathrm{i}^n J_n(x)\mathrm{e}^{\mathrm{i}n\phi} \tag{2.10}$$

where $J_n(x)$ are Bessel functions of the first kind, equation (2.9) can be written as

$$A_{mm'}(\bar{q}_{xy}) = \mathrm{i}^{m'-m}J_{m'-m}(q_{xy}R)\mathrm{e}^{-\mathrm{i}(m'-m)\phi_0}. \tag{2.11}$$

From the above equation, it is obvious that $A_{mm'}$ depends on the difference $\Delta m = m' - m$ only, thus allowing us to write

$$A_{\Delta m}(\bar{q}_{xy}) = \mathrm{i}^{\Delta m}J_{\Delta m}(q_{xy}R)\mathrm{e}^{-\mathrm{i}\Delta m\phi_0}. \tag{2.12}$$

Combining equations (2.1)–(2.3) and (2.8), we have

$$V(\boldsymbol{q}) = \frac{8\pi e^2}{\epsilon q^2}\sum_{\bar{G}}V(\boldsymbol{q}+\boldsymbol{G})\sum_{mm'}A^*_{\Delta m}(\bar{q}_{xy}+\bar{G})A_{\Delta m}(\bar{q}_{xy})\sum_{\boldsymbol{k}}\frac{f_{a'}-f_a}{E_{a'}-E_a+\hbar\omega}. \tag{2.13}$$

Here $\boldsymbol{G} = (\bar{G}, 0)$.

If we define

$$W_{\Delta m}(\boldsymbol{q}) = \sum_{\bar{G}}V(\boldsymbol{q}+\boldsymbol{G})A^*_{\Delta m}(\bar{q}_{xy}+\bar{G}) \tag{2.14}$$

equation (2.13) can be written as

$$V(\boldsymbol{q}) = \frac{8\pi e^2}{\epsilon q^2}\sum_{mm'}W_{\Delta m}(\boldsymbol{q})A_{\Delta m}(\bar{q}_{xy})\sum_{\boldsymbol{k}}\frac{f_{a'}-f_a}{E_{a'}-E_a+\hbar\omega}. \tag{2.15}$$

Since $W_{\Delta m}(\boldsymbol{q}+\boldsymbol{G}) = W_{\Delta m}(\boldsymbol{q})$, from equation (2.15) we have

$$V(\boldsymbol{q}+\boldsymbol{G}) = \frac{8\pi e^2}{\epsilon|\boldsymbol{q}+\boldsymbol{G}|^2}\sum_{mm'}W_{\Delta m}(\boldsymbol{q})A_{\Delta m}(\bar{q}_{xy}+\bar{G})\sum_{\boldsymbol{k}}\frac{f_{a'}-f_a}{E_{a'}-E_a+\hbar\omega}. \tag{2.16}$$

If we multiply equation (2.16) by $A^*_{\Delta m'}(\bar{q}_{xy}+\bar{G})$ and then sum over $\bar{G}$, we get

$$W_{\Delta m'}(\boldsymbol{q}) = \sum_{mm'} W_{\Delta m}(\boldsymbol{q}) \sum_{\bar{G}} \frac{8\pi e^2}{\epsilon|\boldsymbol{q}+\boldsymbol{G}|^2} A^*_{\Delta m'}(\bar{q}_{xy}+\bar{G}) A_{\Delta m}(\bar{q}_{xy}+\bar{G}) \sum_{k} \frac{f_{a'}-f_a}{E_{a'}-E_a+\hbar\omega}. \tag{2.17}$$

The summation of $m$ and $m'$ in equation (2.17) can be replaced by the summation over $\Delta m$ and $m$, hence

$$W_{\Delta m'}(\boldsymbol{q}) = \sum_{\Delta m} W_{\Delta m}(\boldsymbol{q}) \sum_{\bar{G}} \frac{4\pi e^2}{\epsilon|\boldsymbol{q}+\boldsymbol{G}|^2} A^*_{\Delta m'}(\bar{q}_{xy}+\bar{G}) A_{\Delta m}(\bar{q}_{xy}+\bar{G}) P_{\Delta m}(q_z,\omega) \tag{2.18}$$

where

$$P_{\Delta m}(q_z,\omega) = 2\sum_{k,m} \frac{f_{k_z+q_z,m+\Delta m}-f_{k_z,m}}{E_{k_z+q_z,m+\Delta m}-E_{k_z,m}+\hbar\omega}. \tag{2.19}$$

Equation (2.18) implies that the plasmon modes are determined by the zeros of the dielectric matrix

$$\varepsilon_{\Delta m,\Delta m'} = \delta_{\Delta m,\Delta m'} - P_{\Delta m}(q_z,\omega) Q_{\Delta m,\Delta m'}(\boldsymbol{q}) \tag{2.20}$$

where

$$\begin{aligned} Q_{\Delta m,\Delta m'}(\boldsymbol{q}) &= \sum_{\bar{G}} \frac{4\pi e^2}{\epsilon|\boldsymbol{q}+\boldsymbol{G}|^2} A^*_{\Delta m'}(\bar{q}_{xy}+\bar{G}) A_{\Delta m}(\bar{q}_{xy}+\bar{G}) \\ &= \sum_{\bar{G}} \frac{4\pi e^2}{\epsilon|\boldsymbol{q}+\boldsymbol{G}|^2} \mathrm{i}^{\Delta m-\Delta m'} J_{\Delta m}(|\bar{q}_{xy}+\bar{G}|R) J_{\Delta m'}(|\bar{q}_{xy}+\bar{G}|R) \mathrm{e}^{\mathrm{i}(\Delta m'-\Delta m)\phi_0(\bar{q}_{xy}+\bar{G})}. \end{aligned} \tag{2.21}$$

We note that

$$Q_{\Delta m',\Delta m}(\boldsymbol{q}) = Q^*_{\Delta m,\Delta m'}(\boldsymbol{q}). \tag{2.22}$$

Equation (2.20) for a lattice of nanotubes is to be compared to the following equation for the case of a single nanotube [6, 8]:

$$\varepsilon_{\Delta m,\Delta m'} = \delta_{\Delta m,\Delta m'}\left[1 - P_{\Delta m}(q_z,\omega)\frac{\pi e^2}{\epsilon} I_{\Delta m}(q_z R) K_{\Delta m}(q_z R)\right], \tag{2.23}$$

where $I_{\Delta m}$ and $K_{\Delta m}$ are modified Bessel functions of the first and second kind respectively, and $P_{\Delta m}(q_z,\omega)$ has the same form as (2.19) except that $\boldsymbol{k}$ is replaced by $k_z$.

The property of $Q_{\Delta m,\Delta m'}(\boldsymbol{q})$ in the long wavelength limit $q \to 0$ is of special interest. If $n$ represents the highest rotation symmetry axis of the 2D lattice, then the summation over $\bar{G} \neq 0$ terms in equation (2.21) vanishes when $(\Delta m' - \Delta m)/n$ is not an integer, and $Q_{\Delta m,\Delta m'}(\boldsymbol{0})$ is equal to the $\bar{G} = 0$ term only. Making use of the fact that for $\Delta m > 0$ and $x \to 0$,

$$J_{\Delta m}(x) \longrightarrow \frac{1}{(\Delta m)!}\left(\frac{x}{2}\right)^{\Delta m} \tag{2.24}$$

we have

$$\begin{aligned} Q_{\Delta m',\Delta m}(\boldsymbol{0}) = (-1)^{(|\Delta m|-\Delta m+|\Delta m'|-\Delta m')/2} \frac{4\pi e^2 \mathrm{i}^{\Delta m-\Delta m'}}{\epsilon|\Delta m|!|\Delta m'|!}\left(\frac{R}{2}\right)^{|\Delta m|+|\Delta m'|} \\ \lim_{q\to 0} \frac{q_{xy}^{|\Delta m|+|\Delta m'|}}{q^2} \mathrm{e}^{\mathrm{i}(\Delta m'-\Delta m)\phi(\bar{q}_{xy})} \end{aligned} \tag{2.25}$$

when $(\Delta m' - \Delta m)/n$ is not an integer.

## 3. Results

Equation (2.23) tells us that, for a single nanotube, the dielectric matrix has only diagonal elements, namely plasmon modes corresponding to different $\Delta m$ are decoupled. In contrast, the dielectric matrix in equation (2.20) for a lattice of nanotubes is no longer diagonal; the azimuthal symmetry is broken by intertube Coulomb coupling in the lattice and hence the plasmon modes with different $\Delta m$ are now coupled to each other.

Equation (2.19) can be evaluated at zero temperature to give

$$P_{\Delta m}(q_z,\omega)=\frac{m^*}{\pi\hbar^2 q_z a_u}\sum_m \ln\frac{(\hbar\omega_{-m}+E_{\Delta m}+\frac{\hbar^2 m\Delta m}{m^*R^2})^2-(\hbar\omega)^2}{(\hbar\omega_{+m}+E_{\Delta m}+\frac{\hbar^2 m\Delta m}{m^*R^2})^2-(\hbar\omega)^2} \tag{3.1}$$

where $a_u$ is the area of a 2D unit cell, and

$$\hbar\omega_{\pm m}=\frac{(\hbar q_z)^2}{2m^*}\pm\frac{\hbar^2 q_z k_{F,m}}{m^*} \tag{3.2}$$

with $k_{F,m}$ being the Fermi wavevector for the subband with index $m$, and

$$E_{\Delta m}=\frac{(\hbar\Delta m)^2}{2m^*R^2}. \tag{3.3}$$

As is obvious from equation (2.7), subbands with azimuthal indices $\pm m$ are degenerate and have the same Fermi wavevector, $k_{F,-m}=k_{F,m}$. In deriving equation (3.1), we have used the fact that the single particle energy in equation (2.7) is even in $k_z$ and $m$, hence a transformation from $k_z$ to $-k_z$ or from $m$ to $-m$ leaves the expression unchanged. It can be shown that $P_{\Delta m}(q_z,\omega)$ is even in $\Delta m$, i.e.,

$$P_{-\Delta m}(q_z,\omega)=P_{\Delta m}(q_z,\omega). \tag{3.4}$$

### *3.1. Classical plasmon ($\Delta m=0$ mode)*

The $\Delta m=0$ mode is an intrasubband plasmon mode. According to equation (2.20), the coupling of this mode with other $\Delta m\neq 0$ modes depends on if $P_0(q_z,\omega)Q_{0,\Delta m}(\boldsymbol{q})$ vanishes or not. In the long wavelength limit, $P_0(q_z,\omega)\propto q_z^2$. Since the $\bar{G}=0$ term in $Q_{0,\Delta m}(\boldsymbol{0})$ is given by equation (2.25) and the $\bar{G}\neq 0$ terms are well behaved, we find that $P_0(q_z,\omega)Q_{0,\Delta m}(\boldsymbol{0})=0$ in the long wavelength limit for any $|\Delta m|\neq 0$. Therefore in the long wavelength limit, the $\Delta m=0$ mode is decoupled from all $\Delta m\neq 0$ intersubband plasmon modes, and is determined by the zeros of the diagonal element $\varepsilon_{0,0}$ only. This implies that we can expect the coupling of the classical plasmon to $\Delta m\neq 0$ modes to be small for small wavevector $\boldsymbol{q}$ at least.

For finite wavevector $\boldsymbol{q}$, in the diagonal approximation, i.e. we ignore the coupling to $\Delta m\neq 0$ modes, the $\Delta m=0$ intrasubband plasmon frequency $\omega$ is determined by the equation

$$P_0(q_z,\omega)Q_{0,0}(\boldsymbol{q})=1. \tag{3.5}$$

Equation (3.5) is equivalent to

$$\prod_m\frac{(\hbar\omega_{-m})^2-(\hbar\omega)^2}{(\hbar\omega_{+m})^2-(\hbar\omega)^2}=\mathrm{e}^{B_0(\boldsymbol{q})} \tag{3.6}$$

where

$$B_0(\boldsymbol{q})=\frac{\pi\hbar^2 q_z a_u}{m^*Q_{0,0}(\boldsymbol{q})}. \tag{3.7}$$

We can demonstrate that under the right conditions, equation (3.6) gives the classical plasmon formula in 3D, i.e.,

$$\omega^2=\frac{4\pi e^2 n_e}{\epsilon m^*} \tag{3.8}$$

where $n_e$ is the electron density. In the long wavelength limit $q \to 0$, we have $Q_{0,0}(\boldsymbol{q}) \to 4\pi e^2/(\epsilon q^2)$, $\hbar\omega_{\pm m} \to 0$, $B_{0,0}(\boldsymbol{q}) \to 0$, and $\mathrm{e}^{B_{0,0}(\boldsymbol{q})} \to 1 + B_{0,0}(\boldsymbol{q})$. To lowest order in $q$, equation (3.6) gives

$$1 + \frac{1}{(\hbar\omega)^2} \sum_m [(\hbar\omega_{+m})^2 - (\hbar\omega_{-m})^2] = 1 + B_{0,0}(\boldsymbol{q}) \tag{3.9}$$

which leads to the solution

$$\omega^2 = \frac{8e^2 q_z^2}{a_u \epsilon m^* q^2} \sum_m k_{F,m}. \tag{3.10}$$

On the other hand, the electron density $n_e$ is given by

$$n_e = \frac{2}{a_u \pi} \sum_m k_{F,m}. \tag{3.11}$$

Combining the above two equations, we obtain the result in equation (3.8) provided $q_z/q = 1$.

This result shows that, in the long wavelength limit, if many subbands are occupied, all $\Delta m = 0$ modes for different subbands combine together to form a single classical plasmon, in this case a 3D plasmon. Unlike the classical plasmon in a 3D electron gas, the classical plasmon in a carbon nanotube bundle is anisotropic and can be excited only along the $q_z$ direction, as indicated by the wavevector dependence in equation (3.10) and the fact that $P_0(q_z, \omega)$ vanishes if $q_z = 0$. This result is related to the fact that we have assumed electrons cannot tunnel between nanotubes. If tunnelling between nanotubes is permitted, the classical plasmon can then be excited in a direction perpendicular to the nanotubes.

In a single nanotube, the intrasubband plasmon is acoustic with the plasmon energy approaching zero logarithmically as $q \to 0$. In comparison, intertube Coulomb coupling makes the intrasubband plasmon in a nanotube bundle become optical.

If only the lowest subband ($m = 0$) is occupied by electrons, we obtain an analytical solution from equation (3.6) for all values of $\boldsymbol{q}$:

$$(\hbar\omega)^2 = \frac{\mathrm{e}^{B_0(q)}(\hbar\omega_{+0})^2 - (\hbar\omega_{-0})^2}{\mathrm{e}^{B_0(\mathbf{q})} - 1}. \tag{3.12}$$

Although in pure carbon nanotube samples many subbands are occupied, it may be possible to achieve a single occupied subband in intercalated samples [30, 31].

Figure 1($a$) shows the dielectric function $\varepsilon_{0,0}$ using parameters from the experiment of [18]. For $E_F = 8$ eV, subbands with $|m| \leqslant 5$ are all occupied by electrons. For comparison, we show in figure 1($b$) the case where only the lowest subband is occupied. In figure 1($b$), although the real part of the dielectric function becomes zero at two locations, the lower energy zero does not correspond to a plasmon mode because the dielectric function has a nonzero imaginary part at that point. The higher energy zero corresponds to the intrasubband plasmon. Comparing figures 1($a$) and ($b$), we can see in figure 1($a$) that the effect of many occupied subbands is to cause additional structures or singularities in the dielectric function, but there is only one intrasubband plasmon, in this case with an energy of 8.1 eV.

Figure 2 shows the intrasubband plasmon dispersion calculated in the diagonal approximation for the case of a hexagonal lattice. The single tube case (dashed curves) and the upper limit for intrasubband single particle excitation are also plotted for comparison. For reference, the measured $\pi$ plasmon dispersion in [18] is shown by black dots. No attempt has been made to match the theoretical curve with the experimental values. In figure 2 the experimental data and the calculated plasmon energy are close in magnitude and both show significant dispersion along the nanotube direction. The dispersion in the calculated result is larger due to the use of the quadratic wavevector dependence in equation (2.7), while in a real carbon nanotube the

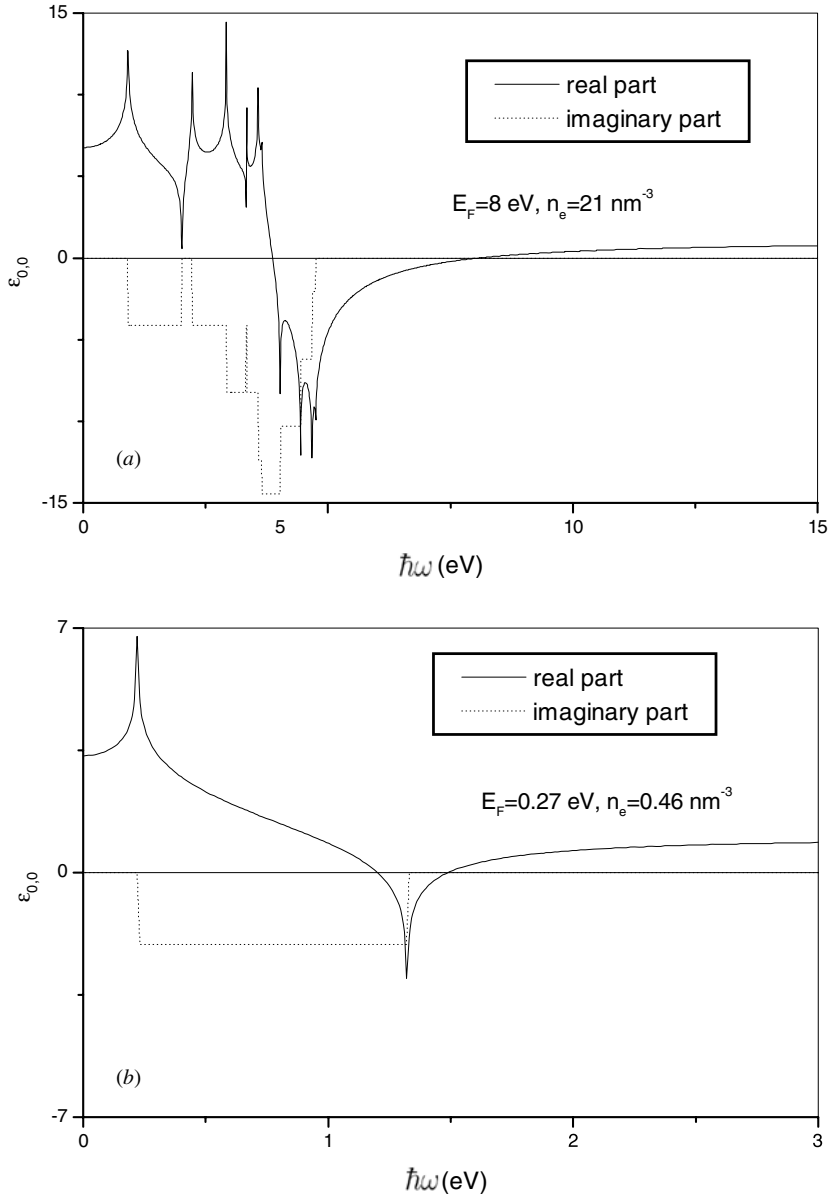


**Figure 1.** Dielectric function $\varepsilon_{0,0}$ for a hexagonal lattice of nanotubes, with nanotube radius $R = 0.7$ nm, lattice constant $b = 1.5$ nm, electron effective mass $m* = 0.277\ m_e$, background dielectric constant $\epsilon = 2.4$, $q_{xy} = 0$, and $q_z = 2\ \text{nm}^{-1}$. In (*a*), all subbands with $|m| \leqslant 5$ are occupied by electrons. In (*b*), only the lowest subband is occupied.

band structure is such that there is less dispersion in electron states. The agreement between theory and experiment is satisfactory considering that the real band structure has not been used in the calculations. The use of the real band structure will be left for future work.

We find in figure 2 that the intrasubband plasmon energies for the hexagonal lattice and a single nanotube are both above the upper limit for intrasubband single particle excitations,

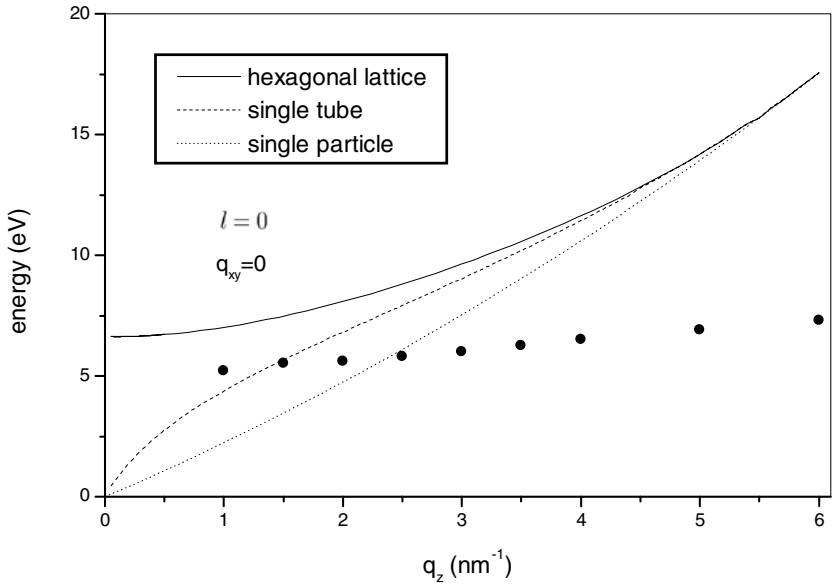


**Figure 2.** Intrasubband plasmon dispersion along $q_z$ for a hexagonal lattice of nanotubes (solid curve) in comparison with the single tube case (dashed curve). The dotted curve is the upper limit for intrasubband single particle excitations. The parameter values are the same as in figure 1(*a*). The black dots are experimental data for the $\pi$ plasmon from [18].

and approach the upper limit for intrasubband single particle excitations asymptotically as $q_z$ increases. This means that intrasubband plasmons in a carbon nanotube system are not damped by single particle type electron–hole pair excitations. The lack of damping is a characteristic of a 1D system. In contrast, the classical plasmon in a 3D electron gas is damped at larger wavevectors.

Figure 2 allows us to compare the plasmon energy of the nanotube bundle with that of a single nanotube. While the intrasubband plasmon in a single nanotube is an acoustic mode, it becomes an optical mode in a nanotube bundle. Intertube Coulomb coupling hardens the intrasubband plasmon at small $q_z$ to make it behave like a 3D plasmon. At large $q_z$, the difference between a nanotube bundle and a single nanotube diminishes. Figure 3 shows the plasmon dispersion in the transverse plane. The abscissa in figure 3 is labeled by points in the hexagonal Brillouin zone. If the real space hexagonal lattice has one of its two basis vectors of length $b$ along the $x$-axis, the reciprocal space lattice is hexagonal with one of its two basis vectors along the $G_y$-axis, and we have $M = (0, \frac{2\pi}{\sqrt{3}b})$ and $K = (\frac{2\pi}{3b}, \frac{2\pi}{\sqrt{3}b})$. For a single nanotube, the plasmon does not have any dispersion in the transverse plane, and a line for the single nanotube plasmon energy is included for comparison purpose. In figure 3, we can see that there is significant dispersion in the transverse plane, and in a large portion of the phase space, the intrasubband plasmon energy of a nanotube bundle is lower than that of a single tube, i.e. intertube Coulomb coupling can also soften the intrasubband plasmon. The role of intertube Coulomb coupling on the plasmon appears to be intricate and fascinating.

Although the single particle energy in equation (2.7) does not have any dispersion in the transverse plane, the intrasubband plasmon in a nanotube bundle is predicted to have a measurable dispersion in the transverse plane. The experimental confirmation of the plasmon dispersion in the transverse plane will provide a good test of the theory.

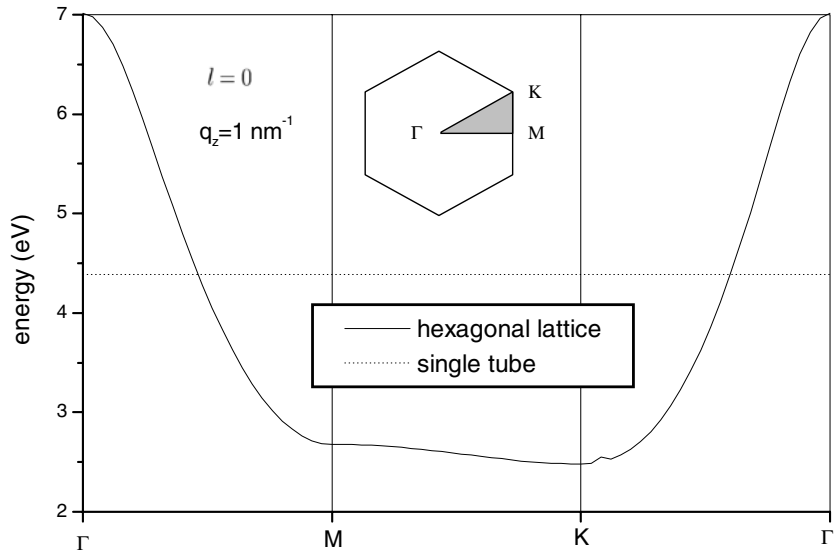


**Figure 3.** Intrasubband plasmon dispersion in the transverse plane for a hexagonal lattice of nanotubes (solid curve) in comparison with the single tube case (dashed curve). The parameter values are the same as in figure 1(*a*).

### *3.2. Quantum plasmons ($\Delta m \neq 0$ modes)*

Quantum plasmons are generally coupled to each other, and some of the intersubband modes are coupled to each other even in the long wavelength limit. In the diagonal approximation where coupling between modes of different $\Delta m$ is neglected, the $\Delta m = \pm l$ modes ($l > 0$) are degenerate like the single nanotube case. To go beyond the diagonal approximation, we consider the pair approximation where the coupling between the $\Delta m = \pm l$ pair of modes is retained but the coupling to other modes are neglected. The rationale is that coupling has the most effect on modes which are close in energy.

It can be shown that the dielectric matrix elements associated with the $\Delta m = \pm l$ modes satisfy the following relations:

$$\varepsilon_{-l,-l} = \varepsilon_{l,l},\ \varepsilon_{-l,l} = \varepsilon^*_{l,-l}. \tag{3.13}$$

In the pair approximation, the coupled pair of $\Delta m = \pm l$ intersubband plasmon modes are determined by the zeros of

$$\det \begin{pmatrix} \varepsilon_{l,l} & \varepsilon_{l,-l} \\ \varepsilon^*_{l,-l} & \varepsilon_{l,l} \end{pmatrix} = 0. \tag{3.14}$$

Equation (3.14) is equivalent to

$$1 - P_l(q_z, \omega)[Q_{l,l}(\boldsymbol{q}) \pm |Q_{l,-l}(\boldsymbol{q})|] = 0. \tag{3.15}$$

If only the lowest subband ($m = 0$) is occupied, we obtain an analytical solution

$$(\hbar\omega)^2 = \frac{\mathrm{e}^{B_{l\pm}(\boldsymbol{q})}(\hbar\omega_{+0} + E_l)^2 - (\hbar\omega_{-0} + E_l)^2}{\mathrm{e}^{B_{l\pm}(\boldsymbol{q})} - 1} \tag{3.16}$$

where

$$B_{l\pm}(\boldsymbol{q}) = \frac{\pi\hbar^2 q_z a_u}{m^*[Q_{l,l}(\boldsymbol{q}) \pm |Q_{l,-l}(\boldsymbol{q})|]} \tag{3.17}$$

and $E_l = \hbar^2 l^2/(2m^* R^2)$ is the single particle energy for an intersubband transition from $m = 0$ to $l$ or $-l$ subbands. In the long wavelength limit, (3.16) reduces to

**Table 1.** List of coupled pair of $\Delta m = \pm l$ modes in the long wavelength limit.

| Lattice type | Coupled pair of $\Delta m = \pm l$ modes in the $q \to 0$ limit |
|---|---|
| Hexagonal lattice | $\Delta m = \pm 1$,[a] |
| | $\Delta m = \pm 3, \pm 6, \pm 9, \ldots$ |
| Square lattice | $\Delta m = \pm 1$,[a] |
| | $\Delta m = \pm 2, \pm 4, \pm 6, \ldots$ |
| All other 2D lattices | $\Delta m = \pm 1, \pm 2, \pm 3, \ldots$ |

[a] Except when $q \to 0$ is achieved along $z$-axis with $q_{xy} = 0$.

$$(\hbar\omega)^2 = E_l^2 + \frac{4E_l k_{F,0}}{\pi a_u}[Q_{l,l}(\mathbf{0}) \pm |Q_{l,-l}(\mathbf{0})|]. \tag{3.18}$$

The second term on the right side of equation (3.18) is the depolarization shift, reflecting the collective nature of the intersubband plasmon. Equation (3.18) indicates that the intersubband plasmons are optical. The presence of $E_l$ in both terms of equation (3.18) indicates that the $\Delta m = \pm l$ intersubband plasmons are reliant on the quantization of the energy levels. For this reason we refer to intersubband plasmons as quantum plasmons.

The two $Q$ factors in equation (3.18) determine the depolarization shift. One can show that $Q_{l,l}(\mathbf{0})$ is always positive and the depolarization shift term is never negative. When the second $Q$ factor $Q_{l,-l}(\mathbf{0})$ vanishes, the $\Delta m = \pm l$ modes are decoupled and degenerate in the long wavelength limit. Whether or not $Q_{l,-l}(\mathbf{0})$ vanishes depends on the lattice type and the value of $l$. There are five Bravais lattices in 2D, with $n$-fold rotation symmetry axes as follows: hexagonal lattice ($n = 6$), square lattice ($n = 4$), primitive rectangular, centred rectangular, and oblique lattices ($n = 2$). From equation (2.25), we see that for $l > 1$, $Q_{l,-l}(\mathbf{0}) = 0$ if $2l/n$ is not an integer, while for $l = 1$, $Q_{l,-l}(\mathbf{0}) \neq 0$ as long as $q_{xy}/q \neq 0$. Therefore, for $l > 1$, the $\Delta m = \pm l$ modes are coupled to each other in the long wavelength limit only if $2l/n$ is an integer. For the $\Delta m = \pm 1$ modes, their coupling not only depends on the lattice type, but also on how the long wavelength limit is achieved. If $q_{xy}/q \neq 0$ when $q \to 0$, the $\Delta m = \pm 1$ modes are coupled to each other for any lattice in the long wavelength limit. If $q_{xy}/q = 0$ when $q \to 0$, the $\Delta m = \pm 1$ modes are decoupled for a hexagonal lattice or square lattice, while for other lattice types they are coupled in the long wavelength limit. Table 1 lists the coupled pair of $\Delta m = \pm l$ modes in the long wavelength limit for all 2D lattice types.

Equation (3.18) can be compared to the single nanotube case,

$$(\hbar\omega)^2 = E_l^2 + \frac{2e^2 E_l k_{F,0}}{l\epsilon}. \tag{3.19}$$

Equation (3.19) was derived from equation (2.23) by taking the long wavelength limit, and noting that when $|\Delta m| = l \neq 0$ and $q_z \to 0$, $I_{\Delta m}(q_z R)K_{\Delta m}(q_z R) \to 1/(2l)$, and $P_{\Delta m}(q_z, \omega) \to (4k_{F,0}E_l/\pi)/[(\hbar\omega)^2 - E_l^2]$ when only the lowest subband is occupied.

We can study the significance of intertube coupling by taking the ratio of the depolarization shift terms in equations (3.18) and (3.19). We find this ratio to be

$$\begin{aligned}\gamma_\pm(l) &= \frac{8l}{a_u}\lim_{q\to 0}\left[\sum_{\bar{G}}\frac{J_l^2(|\bar{q}_{xy}+\bar{G}|R)}{|\boldsymbol{q}+\boldsymbol{G}|^2} \pm \left|\sum_{\bar{G}}\frac{J_l^2(|\bar{q}_{xy}+\bar{G}|R)\mathrm{e}^{-\mathrm{i}2l\phi_0(\bar{q}_{xy}+\bar{G})}}{|\boldsymbol{q}+\boldsymbol{G}|^2}\right|\right] \\ &= \frac{8lR^2}{a_u 4^l}\lim_{q\to 0}\left[\delta_{l,1}\sin^2\theta + \sum_{\bar{G}\neq 0}\frac{4^l J_l^2(GR)}{(GR)^2}\right. \\ &\quad \left. \pm \left|\delta_{l,1}\sin^2\theta\mathrm{e}^{-\mathrm{i}2l\phi_0(\bar{q}_{xy})} + \sum_{\bar{G}\neq 0}\frac{4^l J_l^2(GR)\mathrm{e}^{-\mathrm{i}2l\phi_0(\bar{G})}}{(GR)^2}\right|\right]\end{aligned} \tag{3.20}$$

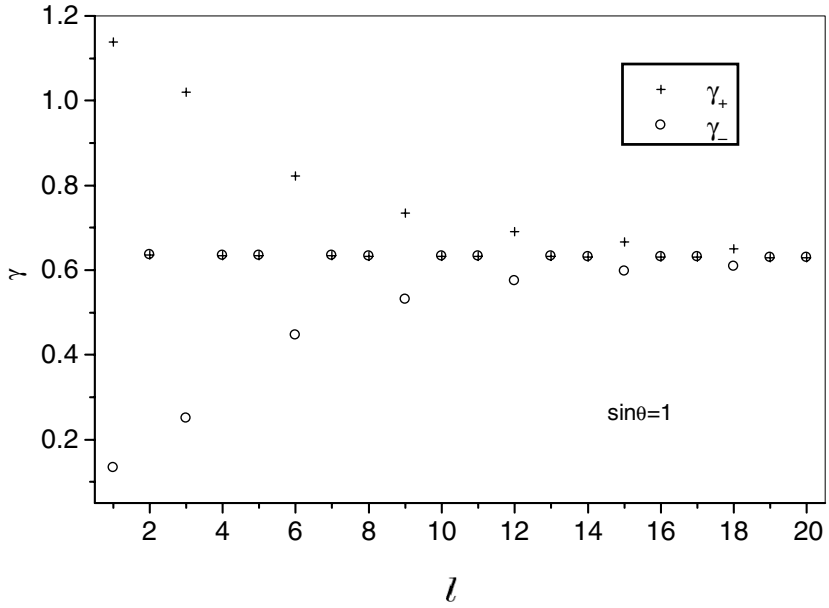


**Figure 4.** $\gamma_{\pm}$ as a function of $l$ for a hexagonal lattice of nanotubes. $\gamma$ greater (less) than one implies the hardening (softening) of the mode near $\Gamma$ point. Parameters used: $R = 0.7$ nm, $b = 1.5$ nm, and $\sin\theta = 1$.

where $\sin\theta = q_{xy}/q$. Figure 4 shows the $\gamma_{\pm}(l)$ values for $l$ up to 20. For the hexagonal lattice, $\gamma_{+}(l)$ and $\gamma_{-}(l)$ are different for $l = 1$, 3, and multiples of three, but the difference becomes smaller as $l$ increases. Interestingly, for those degenerate modes, $\gamma_{\pm}(l)$ values stay essentially constant at 0.63, suggesting that these modes are softened by intertube Coulomb coupling by the same amount in the long wavelength limit. For $l > 3$ all $\gamma$ values in figure 4 are $<1$, which means that intertube Coulomb coupling softens higher $l$ intersubband plasmons in the long wavelength limit. Interestingly, intertube Coulomb coupling softens both the $l = 2$ and 4 modes but hardens one of the $l = 3$ mode in figure 4. For $l = 1$, equation (3.20) implies that the intersubband plasmon can either be hardened or softened depending on the value of $\sin\theta$.

Figure 5 shows the dispersions along $q_z$ of the quantum plasmons with $\Delta m = \pm 1, \pm 2$. The $\Delta m = \pm 1$ modes are degenerate, and so are $\Delta m = \pm 2$ modes. Contrary to the case in figure 2, these modes are lower in energy than the corresponding modes in a single nanotube. In the limit of $q_z = 0$, the $\Delta m = 1$ and 2 plasmons approach energies of 3.37 and 7.86 eV, respectively. The upper limits for $\Delta m = 1$ and 2 single particle excitations at $q_z = 0$ are 0.39 and 1.23 eV, respectively. This means that at $q_z = 0$, there is a huge depolarization shift between single particle intersubband excitations and the corresponding quantum plasmons. This property is reminiscent of the large depolarization shift for quantum plasmons in semiconductor quantum wire superlattices [25, 26].

Figure 6 shows the dispersions of the $\Delta m = \pm 1$ plasmons in the transverse plane. Near the $M$ point the upper branch of the two modes is higher in energy than the mode in a single nanotube, hence intertube Coulomb coupling hardens this mode near $M$ but softens it near $\Gamma$. Similar to the classical plasmon, quantum plasmons also have significant dispersions in the transverse plane. For $q_z \neq 0$, the $\Delta m = \pm 1$ plasmon modes are degenerate at the $\Gamma$ point, while for $q_z = 0$, the $\Delta m = \pm 1$ plasmon modes are split at the $\Gamma$ point (due to the $\sin\theta$ terms in equation (3.20)). The behaviour of the $\Delta m = \pm 1$ modes are singular at the $\Gamma$ point around

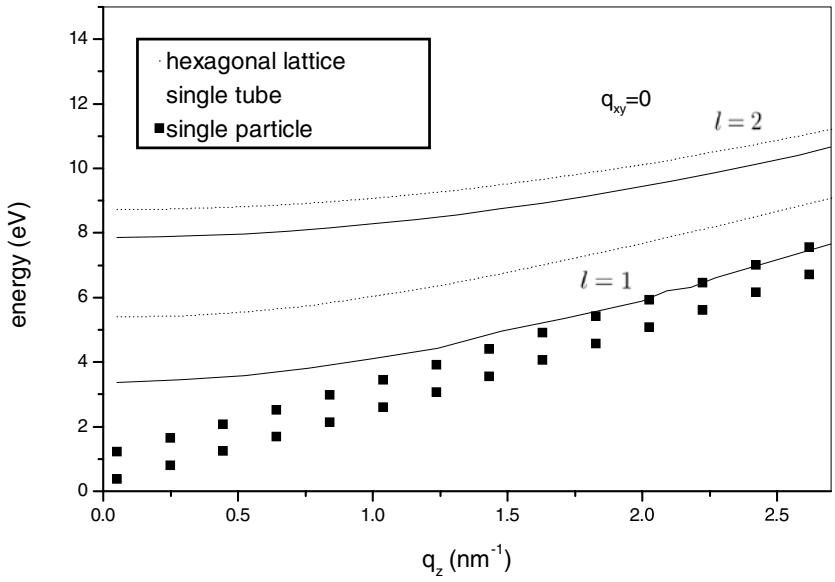


**Figure 5.** Dispersion of the $\Delta m = \pm 1, \pm 2$ intersubband plasmon modes for a hexagonal lattice of nanotubes (solid curves) in comparison with the single tube case (dashed curves). The squares represent the upper limits for $\Delta m = \pm 1, \pm 2$ single particle transition energies. For each pair of curves of the same type, the higher (lower) one corresponds to $\Delta m = \pm 2$ ($\pm 1$). The parameter values are the same as in figure 1(*a*).

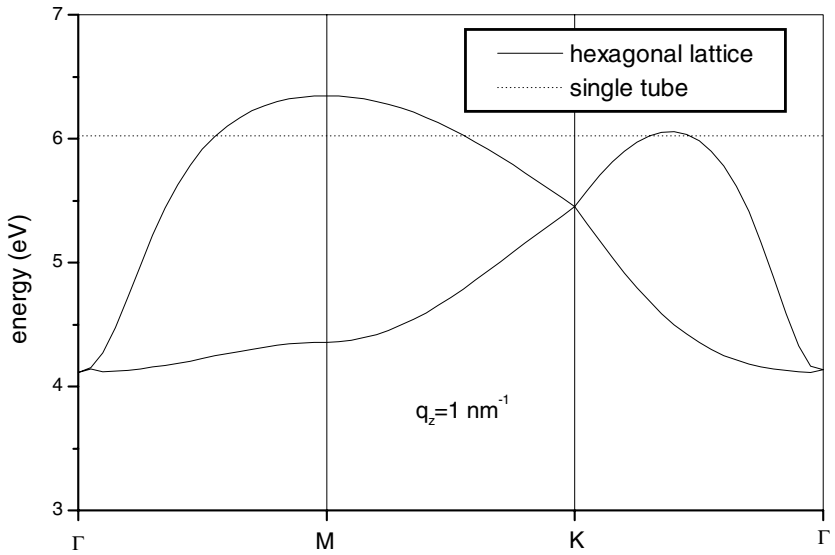


**Figure 6.** Dispersion of the $\Delta m = \pm 1$ intersubband plasmon in the transverse plane for a hexagonal lattice of nanotubes (solid curves) in comparison with the single tube case (dashed curve). The parameter values are the same as in figure 1(*a*).

$q_z = 0$, as suggested by equation (3.20). This singularity is absent in other intersubband or intrasubband modes.

## 4. Discussion

In this paper we have used the pair approximation and neglected coupling to modes outside the pair. In the long wavelength limit, the $\Delta m = l$ ($l \neq 0$) mode is also coupled to $\Delta m = in + l$ modes with $i$ being a nonzero integer and $n$ the rotation symmetry of the lattice. For finite wavevectors, there is coupling to even more modes. Effects of such coupling remain to be explored in future studies.

We have used a conventional electron gas model to describe single particle states in a carbon nanotube. Several authors have suggested that electronic states in carbon nanotubes are not described by Fermi-liquid theory, but by Luttinger-liquid theory [32–34]. Because of this, the study of plasmons in carbon nanotubes may require an entirely different theory. However, in that case the development of the present theory is still valuable, because it will allow a comparison between two types of fundamentally different theories.

A common feature of all quantum plasmons and the classical plasmon is that the plasmon curves do not cross the upper limit for the corresponding single particle excitations, hence the plasmons are not damped by the corresponding single particle electron–hole pair excitations.

The theoretical framework developed here can be applied to more complicated models for carbon nanotubes instead of the free electron gas model, such that the real energy spectra of carbon nanotubes can be used. While the quantitative results will change, the qualitative features predicted based on the simple model are expected to survive.

## Acknowledgments

This work was supported by the Natural Sciences and Engineering Research Council of Canada.

## References

[1] Iijima S 1991 *Nature* **354** 56
[2] Dekker C 1999 *Phys. Today* **52** 22
[3] Baughman R H *et al* 1999 *Science* **284** 1340
[4] Tans S J, Verschueren A R M and Dekker C 1998 *Nature* **393** 49
[5] Li J, Papadopoulos C, Xu J M and Moskovits M 1999 *Appl. Phys. Lett.* **75** 367
[6] Sato O, Tanaka Y, Kobayashi M and Hasegawa A 1993 *Phys. Rev.* B **48** 1947
[7] Davids P S, Wang L, Saxena A and Bishop A R 1994 *Phys. Rev.* B **49** 5682
[8] Lin M F and Shung W K 1993 *Phys. Rev.* B **47** 6617
Lin M F and Shung W K 1994 *Phys. Rev.* B **50** 17 744
[9] Lin M F, Chuu D S, Huang C S, Lin Y K and Shung K W 1996 *Phys. Rev.* B **53** 15 493
[10] Longe P and Bose S M 1993 *Phys. Rev.* B **48** 18 239
[11] Yannouleas C, Bogacheck E N and Landman U 1994 *Phys. Rev.* B **50** 7977
[12] Lin M F and Shung W K 1993 *Phys. Rev.* B **48** 5567
[13] Lin-Chung P J and Rajagopal A K 1994 *Phys. Rev.* B **49** 8454
[14] Davids P S, Wang L, Saxena A and Bishop A R 1995 *Phys. Rev.* B **51** 4557
[15] Bursill L A, Stadelmann P A, Peng J L and Prawer S 1994 *Phys. Rev.* B **49** 2882
[16] Ajayan P M, Iijima S and Ichihashi T 1993 *Phys. Rev.* B **47** 6859
[17] Kuzuo R, Terauchi M and Tanaka M 1992 *Japan. J. Appl. Phys.* **31** L1484
[18] Knupfer M, Pichler T, Golden M S, Fink J, Rinzler A and Smalley R E 1999 *Carbon* **37** 733
[19] Lin M F, Shyu F L and Chen R B 1999 *Phys. Lett.* A **253** 88
[20] Lin M F and Shyu F L 1999 *Phys. Lett.* A **259** 158
[21] Shyu F L and Lin M F 1999 *Phys. Rev.* B **60** 14 434
[22] Shyu F L, Lin M F and Lu Y T 1999 *J. Phys. Soc. Japan* **68** 3352
[23] Lin M F and Chuu D S 1998 *Phys. Rev.* B **57** 10 183

[24] Huang C S, Lin M F and Chuu D S 1999 *J. Phys. Soc. Japan* **67** 2522
[25] Que W and Kirczenow G 1988 *Phys. Rev.* B **37** 7153
Que W and Kirczenow G 1989 *Phys. Rev.* B **39** 5998
[26] Li Q and Das Sarma S 1990 *Phys. Rev.* B **41** 10 268
Li Q and Das Sarma S 1991 *Phys. Rev.* B **43** 11 768
[27] Ostling D, Tomanek D and Rosen A 1997 *Phys. Rev.* B **55** 13 980
[28] Ehrenreich H and Cohen M H 1959 *Phys. Rev.* **115** 786
[29] Que W and Kirczenow G 1988 *Phys. Rev.* B **38** 3614
[30] Lee R S, Kim H J, Fischer J E, Thess A and Smalley R E 1997 *Nature* **388** 255
[31] Rao A M, Eklund P C, Bandow S, Thess A and Smalley R E 1997 *Nature* **388** 257
[32] Brockrath M *et al* 1999 *Nature* **397** 598
[33] Kane C L, Balents L and Fischer M P A 1997 *Phys. Rev. Lett.* **79** 5086
[34] Egger R and Gogolin A O 1997 *Phys. Rev. Lett.* **79** 5082